Quantum theory of terahertz conductivity of semiconductor nanostructures

T. Ostatnický,[1,*] V. Pushkarev,[2] H. Němec,[2] and P. Kužel[2]
[1]*Faculty of Mathematics and Physics, Charles University, Ke Karlovu 3, 12116 Prague 2, Czech Republic*
[2]*Institute of Physics ASCR, Na Slovance 2, 18221 Prague 8, Czech Republic*

(Received 23 June 2017; revised manuscript received 29 January 2018; published 20 February 2018)

Efficient and controlled charge carrier transport through nanoelements is currently a primordial question in the research of nanoelectronic materials and structures. We develop a quantum-mechanical theory of the conductivity spectra of confined charge carriers responding to an electric field from dc regime up to optical frequencies. The broken translation symmetry induces a broadband drift-diffusion current, which is not taken into account in the analysis based on Kubo formula and relaxation time approximation. We show that this current is required to ensure that the dc conductivity of isolated nanostructures correctly attains zero. It causes a significant reshaping of the conductivity spectra up to terahertz or multiterahertz spectral ranges, where the electron scattering rate is typically comparable to or larger than the probing frequency.

DOI: 10.1103/PhysRevB.97.085426

I. INTRODUCTION

Understanding the ultrafast transport of charge carriers in a nanoelement is crucial for the conception and development of nanoelectronic devices [1–4] with target applications in solar cells, photodetector arrays, light-emitting devices like nanoscale lasers, nanotransistors, etc. Currently, several modern instruments can provide various kinds of useful information on the nanoscale conductivity. For example, a dc current flowing through a nanocontact into a sample can be measured using conductive AFM [5]; this experiment provides a map of the conductivity variation (in relative units) over an area on the sample surface. A relative conductivity map in the terahertz or multiterahertz range with subpicosecond time resolution can be obtained using scattering-type near-field scanning optical microscopy [6]. Finally, time and frequency resolved conductivity in large ensembles of nanoobjects can be measured without electrical contacts using the far-field terahertz spectroscopy; such spectra, due to the high probing frequency, carry information on charge transport on nanometer distances [7–9]. Since various transport mechanisms have different spectral fingerprints [10], a broadband spectroscopy has the potential to fundamentally refine the view on charge transport processes.

Quite surprisingly, in many cases the challenge is not the measurement itself, but the lack of theoretical insight, which would allow quantitative microscopic interpretation of the measured spectra. The difficulty is caused by the complexity of an interacting many-particle system which requires fundamental simplifications. On the one hand, calculations of the optical response of solids including nanocrystals typically assume weak scattering (i.e., small scattering rate with respect to the frequency of the probing radiation) [7,11,12]; the results are thus valid only in the optical range. On the other hand, in Ref. [13] the response to a THz probe is calculated using vertex corrections where multiple subsequent scattering processes are taken into account. This method is inherently limited to translationally invariant (bulk) systems due to the factorization of the configuration average of two-particle Green's functions. The quantum theory for the crossover region (THz response of nanocrystals) has not been established yet, since the assumptions used in the above limits are not generally fulfilled. In principle, the full set of many-particle microscopic equations can be solved numerically, but such time-demanding simulations have not been reported, yet. In this situation, semiclassical Monte Carlo calculations [14] constitute the state of the art in the interpretation of experiments on a microscopic level. Analysis of many experimental results is carried out on a purely phenomenological level, e.g., by using the Drude-Smith model [15] based on three heuristic parameters, disregarding even the characteristic size of the nanostructure.

We develop a linear theory of the conductive response of charges in nanostructures based on quantum Kubo formula and relaxation time approximation. The general quantum Kubo formula for the equilibrium conductivity tensor within the linear response theory reads [11,13]

$$\sigma_{\alpha\beta}(\omega) = \frac{iNe^2}{m\omega}\delta_{\alpha,\beta} + \frac{1}{\hbar\omega\mathcal{V}}\int_0^\infty e^{i\omega t}\,\mathrm{Tr}(\rho_0[J_\alpha(t), J_\beta(0)])dt. \quad (1)$$

It involves the time autocorrelation function of the components J_α, J_β of the current operator and the equilibrium density matrix ρ_0 (e is the elementary charge, N is the carrier density, and $\mathcal{V}$ is the nanocrystal volume). Assuming a single-particle approximation, where electrons with an effective mass m occupy energy levels $\hbar\omega_k$ with the probabilities f_k, and a Lorentzian spectral line of a finite width γ due to the electron interaction with impurities, phonons, etc., it can be shown that [7,16]

$$\mathrm{Re}\,\sigma_{\alpha\beta} = \frac{\gamma e^2}{\hbar\omega m\mathcal{V}}\sum_{k,l}\frac{f_k - f_l}{m}\frac{\langle l|p_\alpha|k\rangle\langle k|p_\beta|l\rangle}{(\omega+\omega_k-\omega_l)^2+\gamma^2}. \quad (2)$$

*Corresponding author: tomas.ostatnicky@mff.cuni.cz

The imaginary part is then obtained using the Kramers-Kronig relations. This approach features a phenomenologically introduced charge scattering rate γ and allows one to perform the analysis without exact knowledge of all relevant scattering processes in the system; indeed, their individual rates are usually hardly experimentally accessible. The approximation (2) is pertinent in the optical range for investigations of real nanomaterials, which frequently contain defects and exhibit a distribution of properties, such as size, shape, etc. These conditions fundamentally complicate first principle calculations by adding large uncertainties into their inputs and practically disable evaluation of dephasing processes and direct comparison with the experimental results.

However, the shortcoming of the Kubo formula in the relaxation time approximation (2) is that it always yields nonzero conductivity in the dc limit (at $\omega = 0$). Such a result is unphysical in mutually isolated nanocrystals (no permanent current can flow in a dc field) and it follows that the entire low-frequency region is not appropriately described. This cutting-edge situation is encountered particularly with noncontact probing and it urges for a search of effects, which have been neglected.

In this paper we adapt the Kubo formula to account correctly for the relaxation processes in a space with broken translational symmetry. Namely, a broadband drift-diffusion current due to the motion of scattered carriers is identified and included in the model. This approach is of high importance for interpretation of the behavior of localized charge carriers in nanoelectronic circuits for the GHz range and for contactless terahertz and multiterahertz spectroscopies namely in the challenging regimes, in which the mechanisms of spectral broadening are suppressed (i.e., long scattering time, low temperature, narrow size, and shape distribution of nanoparticles). The theory provides the charge response to the *local* probing electric field; for ensembles of nanocrystals, one must also take into account the effective medium aspects, which have been discussed extensively in the past [17–20].

II. MODEL

In this section, we develop a single-electron model of linear ac conductivity, including a contribution of the nonequlibrium electron diffusive motion. We intentionally simplify the model in order to emphasize the role of the diffusion of confined electrons, thus omitting phenomena related to many-body quantum correlations like excitons. As it will be discussed in Sec. III E, these effects can be, indeed, added as an extension to the general concept presented here.

We consider a conduction band electron responding to a probe (terahertz) electric field within the first-order perturbation theory where the electric field intensity is the perturbation parameter. In our model the single-electron state is described by the density matrix, which can be decomposed as follows:

$$\rho(t) = \rho_0 + \rho_{\mathrm{C}}(t) + \rho_{\mathrm{th}}(t), \tag{3}$$

where the first term on the right-hand side is the stationary density matrix related to the initial equilibrium *thermal state* and the other terms describe the electron response to the perturbation, i.e., they are both of the first order in the electric field intensity.

The second term ρ_{C} defines a *coherent regime*, in which spatial correlations of the phase of the electron wave function play the major role in the dynamics. In bulk systems such a term would describe a momentum-conserving electron propagation with the momentum determined by the spatial phase correlations.

The third term ρ_{th} describes a diffusively moving electron which has lost the spatial phase coherence due to the scattering. This introduces the *thermalization regime*, to which the probed electron enters by the first inelastic scattering event. At this moment the electron spatial distribution in the nanocrystal can be significantly shifted with respect to the equilibrium distribution; therefore, all the subsequent inelastic scattering events must result in a thermalization current bringing the system asymptotically back to the equilibrium thermal state.

However, this thermalization current is not included in the Kubo formula within the relaxation time approximation (2). In a spatially homogeneous system the term ρ_{th} does not produce any current since the system is translationally invariant and, consequently, the loss of coherence due to the scattering automatically brings the system back to its equilibrium. The Kubo formula (2) thus describes well the bulk systems, whereas the contribution of ρ_{th} must be taken into account when the spatial confinement takes place.

The above described introduction of the three distinct regimes of the electron motion allows us to simplify greatly the complete set of kinetic equations. This enables mathematically and physically correct solution of the problem and the level of the description of each regime can be chosen with a desired depth of details. Our basic description is as follows:

(i) *The thermal state* (stationary) is described by a density matrix $\rho_0 = \sum_k |k\rangle f_k \langle k|$, diagonal in the basis of the unperturbed Hamiltonian:

$$H_0 = (p^2/2m) + V(\boldsymbol{r}). \tag{4}$$

Here V is the confining potential and the occupation of eigenstates f_k is given by the Fermi-Dirac distribution. The thermal stationary state obeys the equation of motion:

$$\frac{d}{dt}\rho_0 = 0. \tag{5}$$

(ii) *The coherent regime* is described by a perturbed Hamiltonian $H = H_0 + H'$, where the electron interaction with an external terahertz electric field $\boldsymbol{E}(t)$ in the dipole approximation reads

$$H' = -e\boldsymbol{r} \cdot \boldsymbol{E}(t). \tag{6}$$

The perturbation ρ_{C} of the equilibrium density matrix follows the Liouville equation

$$\frac{d}{dt}\rho_{\mathrm{C}} = -\frac{i}{\hbar}[H', \rho_0] - \frac{i}{\hbar}[H_0, \rho_{\mathrm{C}}] - \gamma\rho_{\mathrm{C}}, \tag{7}$$

which can be easily solved in a stationary regime [21]. Unlike in common approaches, the effective scattering rate γ is connected here to a transfer of the electron to the thermalization regime instead of its relaxation back to equilibrium. Indeed, the scattering event itself does not instantaneously redistribute the (inhomogeneous) spatial electron density. The last term in (7) thus acquires the meaning of the rate of losing the spatial phase correlation of the electron wave function and, as shown

in Appendix C, the rate coincides with the Drude scattering rate.

(iii) The thermalization regime involves a coupling between the density matrix elements up to the infinite order due to the electron scattering with impurities, phonons, etc. The scattering process thus cannot be considered as a weak perturbation. The electron dynamics is system specific and can be hardly solved analytically even if the driving Hamiltonian were exactly known. To simplify the description, we reduce the perturbation in the corresponding density matrix $\rho_{\rm th}$ to a spatially inhomogeneous density of electrons $n_{\rm th}$; its dynamics then yields the thermalization current. We choose the diffusion equation as an appropriate transport equation describing the relaxation to the thermal state:

$$\frac{d}{dt}n_{\rm th}=\gamma\sum_{k,l}\langle \boldsymbol{r}|k\rangle\langle k|\rho_{\rm C}|l\rangle\langle l|\boldsymbol{r}\rangle+\underbrace{D\nabla^2 n_{\rm th}+\nabla\cdot\frac{n_{\rm th}\nabla V}{m\gamma}}_{-\nabla\cdot\boldsymbol{j}_{\rm th}}, \quad (8)$$

where D is the diffusion constant rigorously related to the material parameters through the Einstein's relation $D = k_{\rm B}T/(m\gamma)$ in nondegenerated systems; in a degenerated electron gas the term $k_{\rm B}T$ should be replaced by $N(\partial E_{\rm F}/\partial N)$, where N is the electron concentration in the conduction band [22]. Equation (8) has the form of an equation of continuity. The first (source) term at the right-hand side describes the local density of electrons entering the thermalization regime upon a scattering event and the other terms then represent the local source of a thermalization (drift-diffusion) current density $\boldsymbol{j}_{\rm th}$. This current consists of two components: the diffusion current and the drift current of incoherent carriers submitted to the internal potential V. Although the diffusion equation cannot bring a closer picture of underlying microscopic scattering processes, it can still faithfully represent the thermalization current carrying the charges back to the equilibrium distribution.

The above equations (7) and (8) fully determine the dynamics of the system and can be solved analytically. The mean electric current density is calculated as a sum of the current due to electrons in the coherent regime and of the thermalization current:

$$\boldsymbol{j}=\frac{e}{\mathcal{V}}\left[\langle \boldsymbol{p}\rangle/m+\int \boldsymbol{j}_{\rm th}d^3\boldsymbol{r}\right]. \quad (9)$$

Here, the integration is performed over the nanocrystal volume $\mathcal{V}$. The conductivity tensor then reads

$$\sigma_{\alpha\beta}=\sigma_{\rm C}+\sigma_{\rm th}=\frac{e}{\mathcal{V}E_\beta(\omega)}\mathcal{F}\left[\frac{\mathrm{Tr}\,p_\alpha\rho_{\rm C}(t)}{m}-\int_{\mathcal{V}}\left(D\frac{\partial n_{\rm th}(\boldsymbol{r},t)}{\partial x_\alpha}+\frac{n_{\rm th}}{m\gamma}\frac{\partial V}{\partial x_\alpha}\right)d^3\boldsymbol{r}\right], \quad (10)$$

where E_β is a component of the probing field, x_α is a component of the position vector $\boldsymbol{r}$, and $\mathcal{F}$ denotes the Fourier transformation ($t\to\omega$). Equation (10) is a general result valid for nanocrystals of an arbitrary geometry and for electrons moving in an arbitrary potential landscape. Note that the single carrier response function (mobility μ) can be calculated using $\mu=\sigma/(eN)$.

If the internal potential V is flat in the volume of the nanocrystal, the last term in the integral vanishes and the return of the carriers into the equilibrium is only controlled by the diffusion. By setting formally $D=0$ (inconsistently with the Einstein's relation and finite relaxation rate γ), the thermalization current is suppressed and the result reduces to the simplified Kubo formula (2), which merely accounts for the currents due to the coherent electrons. The thermalization term thus constitutes a correction for the multiple electron scattering up to the infinite order but still being of the first order in the electric field intensity.

III. RESULTS AND DISCUSSION

A. Cube-shaped nanocrystals

As an example, we examine the conductivity of isolated semiconductor nanocubes. The system is modeled by an infinitely deep rectangular potential well with $V(\boldsymbol{r})=0$ for $x,y,z\in(0,a)$ and $V(\boldsymbol{r})=\infty$ otherwise. In addition, we assume the conduction band minimum in the Γ point of the Brillouin zone and an isotropic effective mass. This is the case of GaAs, InP, and related semiconductors. We argue in the Supplemental Material [23] that an analogous expression is found also for silicon where contributions from six equivalent conduction band valleys close to the X point with anisotropic electron effective mass should be taken into account. Numerical examples are provided for GaAs: at room temperature the electron effective mass is $0.067m_{\rm e}$, the scattering rate is $\gamma=(1/270)\ \mathrm{fs}^{-1}$, and the corresponding bulk dc mobility is $\mu=7200\ \mathrm{cm}^2/(\mathrm{V\,s})$ [24,25].

Due to the symmetry the conductivity tensor reduces to a scalar number. For simplicity we consider a probing electric field parallel to the x axis. Stationary solutions of (7) and (8) and their substitution into (10) give the resulting conductivity (see Supplemental Material [23] for the derivation):

$$\sigma_{xx}\equiv\sigma=\frac{e^2}{\hbar a^3}\sum_{k,l}\frac{f_k-f_l}{\omega-\omega_{kl}+i\gamma}\times\left[\sum_{n\ \mathrm{odd}}\frac{2D\gamma a S_{kln}x_{kl}}{D\pi^2n^2-i\omega a^2}-i\omega_{kl}|x_{kl}|^2\right],$$
$$S_{kln}=\delta_{k_y,l_y}\delta_{k_z,l_z}(\delta_{n,k_x-l_x}+\delta_{n,l_x-k_x}-\delta_{n,k_x+l_x}), \quad (11)$$

where k,l are multi-indices denoting eigenstates: $k=(k_x,k_y,k_z)$, all positive integers, the same for l. Energies of the states are known to be

$$E_{(k_xk_yk_z)}=\frac{\pi^2\hbar^2\left(k_x^2+k_y^2+k_z^2\right)}{2ma^2}, \quad (12)$$

and the dipole selection rules [see Eq. (A2) in Appendix A] lead to the following transition energies:

$$\hbar\omega_{kl}=\frac{\pi^2\hbar^2\left(k_x^2-l_x^2\right)}{2ma^2}. \quad (13)$$

We stress that the formula (11) provides the correct zero conductivity in the dc limit for isolated nanocrystals; this statement is explicitly demonstrated in Appendix A.

The general behavior of the model is illustrated in Fig. 1 where we plot the microscopic conductivity of a GaAs cube with size $a=1\ \mu$m in the limit of a low electron concentration ($N=10^{16}\ \mathrm{cm}^{-3}$) such that the Fermi energy lies below the system's ground state by more than $k_{\rm B}T$. To understand the

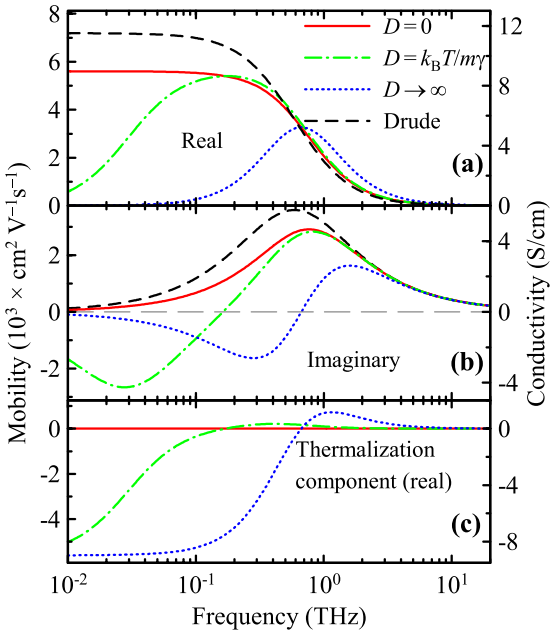

FIG. 1. Calculated (a) real and (b) imaginary conductivity spectra of a GaAs crystal (cubic shape, $a = 1\ \mu$m) for various diffusion coefficients according to (11) at $T = 300$ K and $N = 10^{16}$ cm^{-3}. (c) Real part of the contribution of the thermalization current.

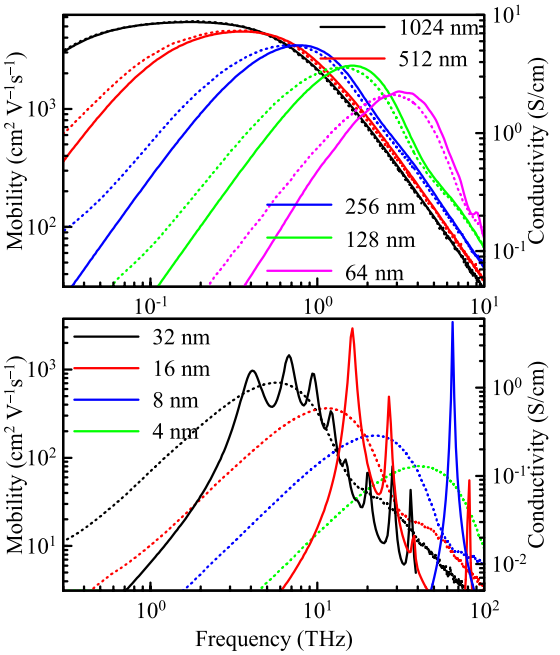

FIG. 2. Comparison of the real parts of conductivities calculated using the quantum model (11) (solid lines) and the semiclassical Monte Carlo method (dotted lines) for selected sizes of large (top panel) and small (bottom panel) nanocubes. $T = 300$ K and $N = 10^{16}$ cm^{-3}.

role of the diffusion, we examine two hypothetical limiting cases:

(1) For $D = 0$ the first term in the square brackets in Eq. (11) vanishes and, in this case, we retrieve the response of electrons with the unphysical nonzero dc conductivity:

$$\sigma_{\mathrm{C}} = -\frac{ie^2}{\hbar a^3}\sum_{k,l}\frac{(f_k - f_l)\omega_{kl}|x_{kl}|^2}{\omega - \omega_{kl} + i\gamma}, \tag{14}$$

equivalent to Eq. (2). The charge confinement only leads to a renormalization of the Drude-like conductivity amplitude due to a lower density of states accessible by optical transitions than in the bulk (Fig. 1).

(2) In the opposite limit ($D \to \infty$) the electrons return to the thermal state immediately after the first scattering event. This overestimates the thermalization current; therefore, the conductivity peak appears at a finite frequency ($\omega \gtrsim \gamma$) even in infinite crystals (i.e., for $a \to \infty$) and the peak amplitude is underestimated. It can be shown (see Appendix B) that this behavior is exactly obtained when the mean electric current density is defined as $\boldsymbol{j} = (e/\mathcal{V})\,(\partial\langle\boldsymbol{r}\rangle/\partial t)$, as it has been done in Ref. [21] [cf. Eqs. (3) and (5) therein]. Although the approximation $D \to \infty$ may greatly simplify the calculations, it is suitable only for small nanocrystals.

As seen in Fig. 1(c), the thermalization current possesses the largest amplitude in the dc regime where it must fully compensate the coherent contribution. Its strength then decreases above the THz spectral range, since the thermalization is a slow process, inefficient at high frequencies.

B. Comparison with the classical Monte Carlo simulations

Any viable quantum model must show a smooth transition to the classical description in the crossover from nano- to micro- or even larger crystals. This is observed in Fig. 2. For the classical calculations we used the Monte Carlo model described in Ref. [14], in which we considered *elastic* collisions of charges with the boundaries of cube-shaped nanoparticles; this is in analogy with the coherent motion of charges in our quantum calculations. The conductivity spectra of micrometer-sized particles calculated using Eq. (11) and the Monte Carlo calculations are practically identical (the classical and quantum curve cannot be distinguished for $a = 1024$ nm in Fig. 2). In Appendix C we show explicitly that Eq. (11) converges to the classical Drude model for an infinitely large crystal; as expected, the thermalization current vanishes for $a \to \infty$.

The top and bottom panels in Fig. 2 represent large and small nanocrystals, respectively. The apparent difference between the two panels is the similarity (top) and difference (bottom) between the overall envelopes of the classical and quantum spectra and, more strikingly, an appearance of the multiple-peak structure in the bottom panel. The crossover between the classical and quantum behavior appears between the sizes 64 nm and 32 nm in the plots. The classical model is expected to fail when the crystal size approaches the electron mean free path $l_{\mathrm{free}} = (1/n)\sum_E g(E)f(E)\sqrt{2E/m\gamma^2}$, where we sum over all discrete electron states with energies E; $g(E)$ is the degeneracy factor, n is the electron number per nanocrystal, and the square root expresses the electron mean free path for the state with the (kinetic) energy E. Considering, for example, $a = 40$ nm, the mean free path of nondegenerate electrons in GaAs at 300 K is $l_{\mathrm{free}} \approx 62$ nm. Indeed, for $a \lesssim l_{\mathrm{free}}$, the quantization effects become important as observed in Fig. 2.

Classical calculations predict a monotonous blueshift of the resonance frequency together with a decrease of its ampli-

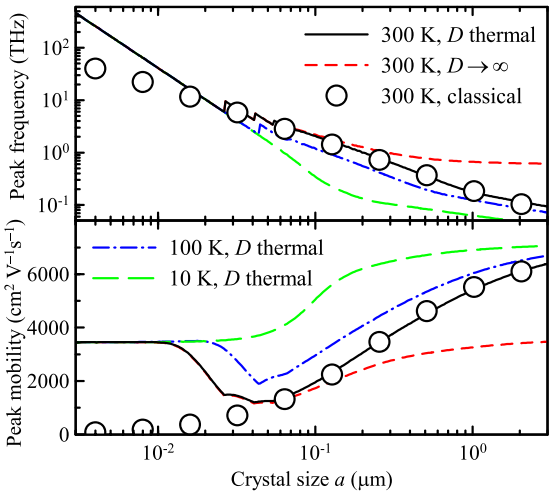

FIG. 3. Frequency (upper panel) and peak value (lower panel) of the main maximum of the real part of the mobility versus the nanocrystal size for GaAs with $N = 10^{16}$ cm^{-3} and $\gamma = (270\ \text{fs})^{-1}$ at all temperatures. Lines: quantum calculations using model (11) at several temperatures for $D = k_B T/(m\gamma)$ or for $D \to \infty$; symbols: classical Monte Carlo calculations [14].

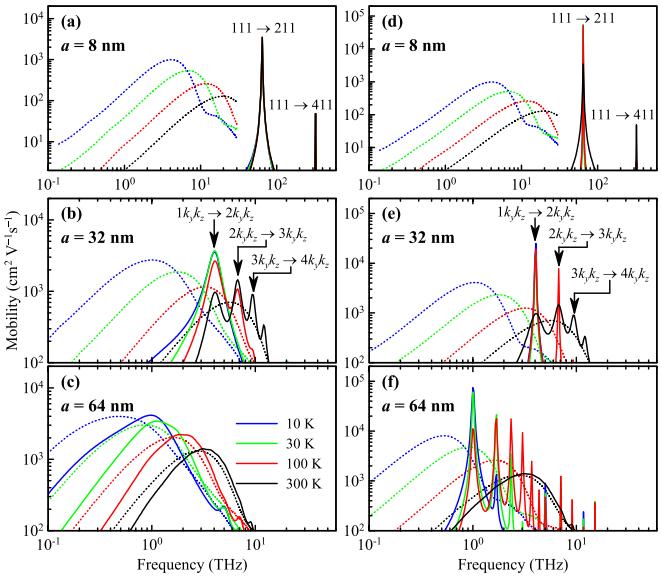

FIG. 4. Comparison of the mobility spectra (real part) of GaAs nanocrystals calculated using the quantum model developed in the manuscript (solid curves) and semiclassical Monte Carlo approach [14] (dotted curves) for (a),(d) small, (b),(e) medium, and (c),(f) large nanocrystals. The conductivity can be calculated using $\sigma\ [\text{S/cm}] \approx \mu\ [\text{cm}^2/(\text{Vs})]/625$. We assume a temperature independent scattering rate $\gamma = (270\ \text{fs})^{-1}$ in (a)–(c). In (d)–(f), the scattering rate is temperature dependent: $\gamma^{-1} = 0.27$, 5.7, 11, and 6.9 ps at 300, 100, 30, and 10 K, respectively (as determined from the mobility measured in Ref. [24]).

tude when the crystal size is reduced (Fig. 3). In quantum calculations the peak frequency shifts with $1/a^2$ for small nanocrystal sizes [this reflects the variation of the energy splitting of quantized levels; see Eq. (13)], while the shift slows down for higher nanocrystal sizes. The agreement between the quantum and classical model is excellent for large nanocrystals at room temperature. The peak conductivity amplitude from the quantum model remains almost constant for very small nanocrystals [26] reflecting invariance of the oscillator strength upon the size scaling as expected from the Thomas-Reiche-Kuhn (TRK) sum rule. In the case of large nanocrystals, where the classical conductivity regime is approached, the effective width of the conductivity peak decreases upon an increase of the nanocrystals size; therefore, following the TRK sum rule, the peak conductivity must increase, too, and it tends to the dc limit of the Drude behavior for any finite D (Fig. 3). The crossover region is connected with the crystal sizes comparable to the electron mean free path.

In small nanocrystals, energy levels are well separated (by more than $k_B T$); therefore, the conductivity spectra contain a series of peaks due to quantum transitions allowed by the dipole coupling (Fig. 2).

Strictly speaking, approximating the thermalization regime by the diffusion equation is valid only for nanocrystal sizes exceeding the electron mean free path. For smaller nanocrystals the ballistic motion takes over: the dynamics of the spatial charge redistribution thus becomes faster and this can be roughly viewed as an enhanced diffusion. However, an increase of the value of D has only little impact for small nanocrystals ($a < l_{\text{free}}$), as illustrated in Fig. 3. This justifies the use of the presented results for any nanocrystal size.

C. Temperature dependences

The temperature dependence of the conductivity spectra predicted by our quantum model is determined by an interplay of several factors: energy levels spacing, spectral broadening due to the dephasing, and appearance of higher-order transitions due to the population of higher levels (with increasing temperature and nanocrystal size). The discrete energy levels due to the quantum interference in an infinite potential well are expressed by Eq. (12), i.e., the spacing between them is inversely proportional to the square of the nanocrystal size.

We discuss the behavior of the mobility (conductivity) spectra side by side for a *temperature independent* and *temperature dependent* scattering rate γ. By assuming the temperature independent γ one can easily discriminate the principal regimes, while $\gamma(T)$ corresponds to physical situations in real materials. We take the case of GaAs with a single type of carrier (electron). The scattering rate in GaAs decreases with decreasing temperature in the range 50–300 K due to a reduced electron-phonon scattering. The ionized impurity scattering takes over at lower temperatures, which means that γ starts to increase with the decreasing temperature below ~50 K [24]. Depending on the size of nanocrystals (and taking into account also the temperature of the system), we can identify three cases.

(1) *Small nanocrystals*; Figs. 4(a) and 4(d).

Temperature independent γ. The separation of energy levels is large; we can then analyze this case in the regime when only the lowest energy level, $E_{(111)}$, is populated in the ground state, i.e., for temperatures $k_B T \ll (E_{(211)} - E_{(111)})$. The selection rules (A2) predict that the system can undergo optical transitions only to levels $E_{(n11)}$, where $n \geqslant 2$ is an even number. The conductivity spectrum consists of a series of temperature independent peaks corresponding to individual transitions with

a peak amplitude decreasing roughly with $1/n^4$ as it can be deduced from Eqs. (13), (14), and (A2). The peaks are sharp when the scattering is sufficiently slow, $\hbar\gamma \ll E_{(111)}$, as illustrated in Fig. 4(a). In contrast, semiclassical Monte Carlo calculations predict a false strong temperature dependence of the conductivity: in this case, the frequency of the maximum of the broad conductivity peak is proportional to the mean carrier velocity (which is temperature dependent: $v_{\mathrm{mean}} = \sqrt{k_{\mathrm{B}}T/m}$); see Fig. 4(a).

Temperature dependent γ. The linewidths of the conductivity peaks scale with the scattering rate, while their amplitudes are inversely proportional to the scattering rate Fig. 4(d). The positions of spectral lines are temperature independent similar to the case of temperature independent γ. Striking discrepancies between the quantum and classical calculations are observed again.

(2) *Medium nanocrystals*; Figs. 4(b) and 4(e).

Temperature independent γ. At low temperatures only the level (111) is populated and the behavior is identical to that of small nanocrystals. With increasing temperature, higher energy levels (211, 311, ...) become populated in the ground state, which opens up new possible optical transitions, e.g., (211) $\rightarrow$ (311), etc. For small or moderate scattering rates these transitions can be resolved in the spectra as individual peaks emerging with increasing temperature; see Fig. 4(b) for illustration. The peak frequencies are defined by the energy difference $E_{(k_x+2n+1,k_y,k_z)} - E_{(k_x,k_y,k_z)}$. Note that this value is independent of the quantum numbers k_y and k_z, i.e., several transitions may contribute to each observed peak. For large scattering rate these peaks cannot be spectrally resolved and will merge into a broad conductivity peak.

Temperature dependent γ. The low-temperature behavior is very similar to that of small nanocrystals: the condition $k_{\mathrm{B}}T \ll E_{(211)} - E_{(111)}$ is still valid. For $T \gtrsim 100$ K higher order transitions appear in the spectra; the spectral lines partly merge at 300 K owing to the increased scattering. Note that at this temperature the position, amplitude, and overall linewidth of the broad spectral feature calculated using the quantum model is comparable to the one obtained by semiclassical Monte Carlo calculations; see Fig. 4(e).

(3) *Large nanocrystals*; Figs. 4(c) and 4(f).

Temperature independent γ. The lowest transition energy $E_{(211)} - E_{(111)}$ is small compared to $k_{\mathrm{B}}T$. In this situation, a large number of the lowest lying energy levels $E_{(k_xk_yk_z)}$ is populated, giving rise to a huge number (quasicontinuum) of allowed transitions. A line broadening caused by the scattering then ensures that all these lines merge into a single broad band. In this limit, the quantum and classical Monte Carlo calculations provide very similar results. Then it is not surprising that a temperature dependence emerges also in the spectra obtained by the quantum calculations: this dependence stems from a variation of the population of individual energy levels as a function of temperature; see Fig. 4(c).

Temperature dependent γ. At room temperature a broadband spectrum is observed and it shows a good agreement with the one calculated by the semiclassical model. At lower temperatures, individual transitions are observed instead of broad bands: this is due to the decrease of the scattering rate leading to very narrow linewidths of individual transitions; see Fig. 4(f).

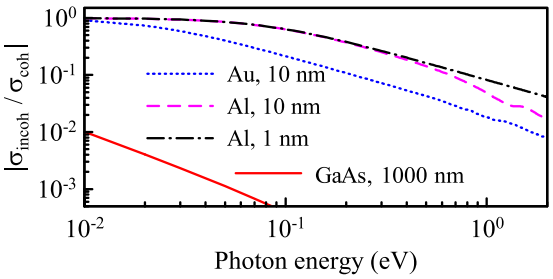

FIG. 5. Relative weight of the thermalization current at 300 K represented by $|\sigma_{\mathrm{incoh}}/\sigma_{\mathrm{coh}}|$ in nanocubes made of GaAs ($N = 10^{16}$ cm^{-3}), Au, and Al calculated for various nanocrystal sizes. The parameters of the metals (plasma frequency, free carrier concentration, and scattering rate) are from Refs. [22,28].

From the above discussion we can draw a general conclusion that the quantum spectra are practically temperature independent as long as the thermal energy is low compared to energy level spacing. Such a behavior is in a sharp contrast with semiclassical calculations, which predict a strong temperature dependence. Since no strong temperature dependence of the conductivity spectra has been observed in real systems composed of small nanocrystals [21,27], the developed quantum calculations are thus indirectly supported.

D. Short note on degenerate systems

Let us compare here the thermalization current in semiconductors with that in degenerate systems such as metallic nanoparticles; see Fig. 5. In weakly or moderately doped GaAs and similar semiconductors the thermalization corrections are significant only up to a few THz at low temperatures or up to the multi-THz spectral range at room temperature. In metals such as Au or Ag with a single valence electron per atom contributing to the metallic conductivity, the thermalization current is significant up to optical frequencies where the motion of incoherent electrons may require a correction as large as several percent (Fig. 5; the response of Ag is very similar to Au). In aluminum with three valence electrons contributing to the conductivity, the diffusion is significantly faster and the thermalization correction is even larger.

E. Applicability and limitations of the model

The conducting carriers in semiconductors may have several origins: doping, thermal excitation, or photoexcitation. In time-resolved photoconductivity experiments the finite carrier lifetime T_1 (i.e., the carrier interband relaxation time) must be also considered and in this case our model requires the condition $1/T_1 \ll \gamma$ which is most frequently valid. Despite several approximations, namely the omission of electron-hole correlations, the model developed in Sec. II may be directly applied in the following cases:

(1) *In doped (nonphotoexcited) nanocrystals* a single type of carrier (electrons or holes) exists and the electron-hole interaction is of no importance.

(2) *In small nanocrystals* with the size smaller than the exciton Bohr radius, the electron-hole correlations are inherently induced by the presence of the confining potential.

The Coulomb correlations therefore renormalize the optical spectra but they are not responsible for any new features. These renormalizations can be estimated within the mean field approximation.

(3) *At high temperatures*, such that $k_B T$ is larger than the exciton ionization energy, no exciton bound states exist in the system and the conductivity can be determined as a sum of the separate electron and hole conductivities.

For nanocrystals with the size exceeding the exciton Bohr radius the applicability of the single-particle electron or hole states is limited: bound electron-hole states do exist. In this case the more appropriate electron-hole quasiparticle wave functions must be used as the basis set of the system. With these precautions our model remains fully applicable.

IV. CONCLUSIONS

In summary, we derived a general analytical formula (10) for microscopic ac electric conductivity of semiconductor (or metallic) nanocrystals, which was analyzed in particular for nanocubes, resulting in the analytical formula for nanocube conductivity (11). Our result consists of the usual Kubo formula corrected by a thermalization current, which accounts for the motion of incoherently scattered charges in systems with broken translational symmetry. We verified that our result correctly reproduces important limits (zero dc conductivity in finite isolated nanocrystals, classical limit, and Drude conductivity in large crystals). The thermalization current is inherent to all confined systems: in nondegenerate electron gases, its influence is significant up to multiterahertz frequencies, while, in metallic nanoparticles, its contribution may persist up to the optical range. The thermalization current also appears in electrical circuits containing nanodevices, which exhibit localized electron states due to tunneling barriers between the nanodevice and the electrical contacts.

ACKNOWLEDGMENTS

We acknowledge the financial support by the Czech Science Foundation (Project No. 17-03662S) and European Union funding under the 7th Framework Programme (Project No. 607521, NOTEDEV).

APPENDIX A: DC CONDUCTIVITY

Here we evaluate the sum over n in Eq. (11) for $\omega = 0$. For any combination of the indices k and l one can find two terms in the sum which contribute: $n = k_x + l_x$ and either $n = k_x - l_x$ or $n = l_x - k_x$, both of them satisfying $n^2 = (k_x - l_x)^2$. We may therefore write the sum in the dc limit as follows:

$$\sum_{n\ \mathrm{odd}} \frac{2D\gamma a S_{kln} x_{kl}}{D\pi^2 n^2 - i\omega a^2}$$

$$= \sum_{n\ \mathrm{odd}} \frac{2\gamma a S_{kln} x_{kl}}{\pi^2 n^2} = \delta_{k_y,l_y}\delta_{k_z,l_z} \times \gamma x_{kl} \frac{a}{\pi^2}\left[\frac{1}{(k_x - l_x)^2} - \frac{1}{(k_x + l_x)^2}\right][1 - (-1)^{k_x+l_x}]. \quad \text{(A1)}$$

Using the standard set of real wave functions (see Eq. (S20) in the Supplemental Material [23]) for the eigenstates of unperturbed Hamiltonian (4), the dipole matrix element x_{kl} is given by the formula

$$x_{kl} = x_{lk} = -\frac{a}{\pi^2}\left[\frac{1}{(k_x - l_x)^2} - \frac{1}{(k_x + l_x)^2}\right] \times [1 - (-1)^{k_x+l_x}]\delta_{k_y,l_y}\delta_{k_z,l_z}. \quad \text{(A2)}$$

It follows that $x_{kl} \in \mathbb{R}$ and thus $x_{kl} = x_{lk}$ and $x_{kl}^2 = |x_{kl}|^2$. After the substitution, we easily find

$$\sigma_{\mathrm{dc}} = \frac{ie^2}{\hbar a^3}\sum_{k,l} \frac{f_{kl}(i\gamma - \omega_{kl})|x_{kl}|^2}{i\gamma - \omega_{kl}} = \frac{ie^2}{\hbar a^3}\sum_{k,l} f_{kl}|x_{kl}|^2 = 0. \quad \text{(A3)}$$

The term f_{kl} is odd with respect to the permutation of indices k and l, while the term $|x_{kl}|^2$ is even and therefore the double sum vanishes.

APPENDIX B: INSTANTANEOUS THERMALIZATION

We set $D \to \infty$ in a crystal with finite dimensions; since $D\pi^2 n^2 \gg \omega a^2$ for $n > 0$, the latter term may be neglected in Eq. (11). We may then rewrite (11) with the help of (A1) and (A2):

$$\sigma_{D\to\infty} = \frac{e^2}{\hbar a^3}\sum_{k,l} \frac{f_{kl}|x_{kl}|^2}{\omega - \omega_{kl} + i\gamma}[-\gamma - i\omega_{kl}] = \frac{ie^2}{\hbar a^3}\sum_{k,l} \frac{f_{kl}|x_{kl}|^2}{\omega - \omega_{kl} + i\gamma}(\omega - \omega_{kl} + i\gamma) - \frac{ie^2\omega}{\hbar a^3}\sum_{k,l} \frac{f_{kl}|x_{kl}|^2}{\omega - \omega_{kl} + i\gamma}. \quad \text{(B1)}$$

The first sum on the right hand side vanishes due to the odd parity of the summand (see the previous section). The second sum is equivalent to the expression which we used previously [21] for calculations of the electron mobility in small nanocrystals. The previously derived formula in Ref. [21] was based on the definition of the mean electric current density $\boldsymbol{j} = (e/\mathcal{V})\,(\partial\langle \boldsymbol{r}\rangle/\partial t)$. This definition takes into account the particle thermalization (the dc current is zero) but apparently the thermalization process is instantaneous after the first scattering event since here we obtain the same expression when setting $D \to \infty$.

APPENDIX C: INFINITE CRYSTAL

We denote

$$\Sigma_{kl} = \sum_{n\ \mathrm{odd}} \frac{2D\gamma a S_{kln}}{D\pi^2 n^2 - \mathrm{i}\omega a^2}\,. \quad \text{(C1)}$$

We sum separately the pairs of terms with exchanged k, l in Eq. (11) and we consider that $x_{kk} = 0$. We obtain

$$\sigma = \frac{2e^2}{\hbar a^3}\sum_{k_x > l_x} \frac{f_{kl}\omega_{kl}x_{kl}}{(\omega + i\gamma)^2 - \omega_{kl}^2}[\Sigma_{kl} - i(\omega + i\gamma)x_{lk}]. \quad \text{(C2)}$$

Here the label of the sum $k_x > l_x$ means sum over all three indices k,l such that $k_x > l_x$. The largest contribution to the

sum comes from the terms $k \approx l$ as it can be inferred from the explicit form of the dipole matrix element (A2); therefore, $n \approx 1$ in Σ_{kl}. For a fixed value of ω we may therefore choose a sufficiently large value of the crystal size such that $\omega a^2 \gg D\pi^2 n^2$ and therefore $\Sigma_{kl} \propto a^{-1}$; the second term in the square brackets in (C2) is directly proportional to a. An increase of the crystal size a leads to an increase of the density of states; as a consequence, the frequency separation ω_{kl} of the states coupled by the dipole transition becomes smaller. To summarize, for a sufficiently large value of a, the term Σ_{kl} may be neglected in the numerator and ω_{kl} may be neglected in the denominator of (C2). Then we get

$$\sigma_{a\to\infty} = -\frac{2ie^2}{\hbar a^3} \sum_{k_x > l_x} \frac{f_{kl}\omega_{kl}|x_{kl}|^2}{\omega + i\gamma}. \tag{C3}$$

Finally, the terms $f_{kl}\omega_{kl}|x_{kl}|^2$ are symmetric with respect to the permutation of indices k and l; moreover, the diagonal terms do not contribute, since $f_{kk} = 0$ and $x_{kk} = 0$. Taking these symmetries into account we finally obtain

$$\sigma_{a\to\infty} = -\frac{ie^2}{\hbar a^3} \sum_{k,l} \frac{f_{kl}\omega_{kl}|x_{kl}|^2}{\omega + i\gamma}. \tag{C4}$$

It can be shown analytically for an arbitrary temperature that this expression tends to the Drude formula for the bulk crystals:

$$\sigma_{\text{Drude}} = \frac{ie^2 N}{m} \frac{1}{\omega + i\gamma}, \tag{C5}$$

where N is the electron density. We may conclude that the effective scattering rate γ coincides with the Drude scattering term which is the inverse of the scattering time [13].

[1] C. J. Docherty and M. B. Johnston, J. Infrared Milli. Terahz. Waves **33**, 797 (2012).

[2] A. Cresti, N. Nemec, B. Biel, G. Niebler, F. Triozon, G. Cuniberti, and S. Roche, Nano. Res. **1**, 361 (2008).

[3] C. R. Kagan and C. B. Murray, Nat. Nanotechnol. **10**, 1013 (2015).

[4] F. Hetsch, N. Zhao, S. V. Kershaw, and A. L. Rogach, Mater. Today **16**, 312 (2013).

[5] M. Lanza, *Conductive Atomic Force Microscope* (Wiley-VCH, Weinheim, 2017).

[6] M. Eisele, T. L. Cocker, M. A. Huber, M. Plankl, L. Viti, D. Ercolani, L. Sorba, M. S. Vitiello, and R. Huber, Nat. Photonics **8**, 841 (2014).

[7] J. Lloyd-Hughes and T.-I. Jeon, J. Infrared Milli Terahz Waves **33**, 871 (2012).

[8] R. Ulbricht, E. Hendry, J. Shan, T. F. Heinz, and M. Bonn, Rev. Mod. Phys. **83**, 543 (2011).

[9] F. A. Hegmann, O. Ostroverkhova, and D. G. Cooke, *Photophysics of Molecular Materials* (Wiley-VCH Verlag GmbH & Co. KGaA, Weinheim, 2006), Chap. 7, pp. 367–428.

[10] H. Němec, P. Kužel, and V. Sundström, J. Photochem. Photobiol. A **215**, 123 (2010).

[11] G. D. Mahan, *Many-particle Physics* (Plenum Publishers, New York, 1981).

[12] H. Haug and S. W. Koch, *Quantum Theory of the Optical and Electronic Properties of Semiconductors* (World Scientific, Singapore, 1990).

[13] H. J. W. Haug and A.-P. Jauho, *Quantum Kinetics in Transport and Optics of Semiconductors* (Springer, Berlin, 1997).

[14] H. Němec, P. Kužel, and V. Sundström, Phys. Rev. B **79**, 115309 (2009).

[15] N. V. Smith, Phys. Rev. B **64**, 155106 (2001).

[16] M. P. Marder, *Condensed Matter Theory* (Wiley, New York, 2000).

[17] H. Němec, V. Zajac, I. Rychetský, D. Fattakhova-Rohlfing, B. Mandlmeier, T. Bein, Z. Mics, and P. Kužel, IEEE T. THz Sci. Technol. **3**, 302 (2013).

[18] H.-K. Nienhuys and V. Sundström, Appl. Phys. Lett. **87**, 012101 (2005).

[19] E. Hendry, M. Koeberg, B. O'Regan, and M. Bonn, Nano Lett. **6**, 755 (2006).

[20] P. Kužel and H. Němec, J. Phys. D **47**, 374005 (2014).

[21] V. Pushkarev, T. Ostatnický, H. Němec, T. Chlouba, F. Trojánek, P. Malý, M. Zacharias, S. Gutsch, D. Hiller, and P. Kužel, Phys. Rev. B **95**, 125424 (2017).

[22] N. W. Ashcroft and N. D. Mermin, *Solid State Physics* (Holt, Rinehart and Winston, New York, 1988).

[23] See T. Ostatnický, V. Pushkarev, H. Němec, and P. Kužel, in Supplemental Material at http://link.aps.org/supplemental/10.1103/PhysRevB.97.085426 for detailed derivation of the conductivity of cube-shaped nanocrystals.

[24] G. E. Stillman, C. M. Waife, and J. O. Dimmock, J. Phys. Chem. Solids **31**, 1199 (1970).

[25] P. Y. Yu and M. Cardona, *Fundamentals of Semiconductors* (Springer, Berlin, 1996).

[26] Note that we calculate the conductivity per unit volume (not per nanocrystal) at constant electron density N.

[27] L. Fekete, P. Kužel, H. Němec, F. Kadlec, A. Dejneka, J. Stuchlík, and A. Fejfar, Phys. Rev. B **79**, 115306 (2009).

[28] M. A. Ordal, L. L. Long, R. J. Bell, S. E. Bell, R. R. Bell, R. W. Alexander, Jr., and C. A. Ward, Appl. Opt. **22**, 1099 (1983).